JGR Biogeosciences

RESEARCH ARTICLE
10.1029/2023JG007466

Methane Emissions From Land and Aquatic Ecosystems in Western Siberia: An Analysis With Methane Biogeochemistry Models

Xuan Xi[1], Qianlai Zhuang[1,2], Seungbum Kim[3], and Zhen Zhang[4,5]

[1]Department of Earth, Atmospheric, and Planetary Sciences, Purdue University, West Lafayette, IN, USA, [2]Department of Agronomy, Purdue University, West Lafayette, IN, USA, [3]NASA Jet Propulsion Laboratory, Pasadena, CA, USA, [4]National Tibetan Plateau Data Center (TPDC), State Key Laboratory of Tibetan Plateau Earth System, Environment and Resource (TPESER), Institute of Tibetan Plateau Research, Chinese Academy of Sciences, Beijing, China, [5]Department of Geographical Sciences, University of Maryland, College Park, MD, USA

Key Points:

- Methane emissions from both land and aquatic ecosystems over Western Siberia are quantified
- Total methane emissions over Western Siberia range from 4.80 ± 0.43 to 8.29 ± 0.81 Tg CH_4/year from 2016 to 2020
- It is important to develop both dynamic wetland and aquatic area data in quantifying regional methane emissions

Supporting Information:

Supporting Information may be found in the online version of this article.

Correspondence to:

Q. Zhuang,
qzhuang@purdue.edu

Citation:

Xi, X., Zhuang, Q., Kim, S., & Zhang, Z. (2023). Methane emissions from land and aquatic ecosystems in Western Siberia: An analysis with methane biogeochemistry models. *Journal of Geophysical Research: Biogeosciences*, *128*, e2023JG007466. https://doi.org/10.1029/2023JG007466

Received 6 MAR 2023
Accepted 27 JUN 2023

Abstract Western Siberia contains extensive wetlands and aquatic ecosystems, contributing a significant amount of methane (CH_4) emissions to the atmosphere. However, estimates of CH_4 fluxes over the region are poorly constrained partly due to the uncertainties from the inundated area data. This study applied two process-based biogeochemistry models to quantify the emissions from land and aquatic ecosystems over the region within the period 2000–2021 using different inundation datasets. To drive land methane modeling, we use one static wetland map and one dynamic wetland area data set called Wetland Area and Dynamics for Methane Modeling (WAD2M) (2000–2020). To drive lake methane modeling, we use the surface area of aquatic ecosystems from three datasets: (a) HydroLAKES; (b) Global Surface Water (GSW); and (c) surface water inundation from Soil Moisture Active Passive (SMAP) (2016–2021). Using these datasets, we conduct four simulations to compare emissions over the region. We find that the net methane emissions from land using the static wetland map are larger than those using WAD2M. SMAP and GSW estimate larger emissions than HydroLAKES does from aquatic ecosystems. Total emissions over the region range from 4.80 ± 0.43 to 8.29 ± 0.81 Tg CH_4/year from 2016 to 2020, which is the intersection period of four simulations. This study is among the first to investigate methane emissions from the whole landscape in the region. Our study highlights the importance of dynamic wetland and aquatic area data in quantifying regional methane emissions.

Plain Language Summary Methane (CH_4) is a vital greenhouse gas that can make large differences in global climate change. In this study, we quantified total methane emissions over Western Siberia, which is a methane-emitting hotpot. We used two process-based models to quantify methane emissions from both land and aquatic ecosystems over the region. We used different combinations of wetlands and aquatic areal datasets to run four model simulations for comparison. We found that the total emissions over the region range from 4.80 ± 0.43 to 8.29 ± 0.81 Tg CH_4/year from 2016 to 2020 depending on the land and aquatic areal dynamics. We conclude that it is important to develop dynamic wetland and aquatic area data in quantifying regional methane emissions.

1. Introduction

Since the industrial age, methane (CH_4), as the second-largest greenhouse gas behind carbon dioxide (CO_2), has accounted for 20% of the observed warming (Ciais et al., 2013). Furthermore, since methane emission is closely related to the increasing temperature at present, it is important to quantify methane emissions under a changing climate (Walter et al., 2001; Zhuang et al., 2013). The natural sources of methane mainly include vegetated wetlands, inland aquatic ecosystems (lakes, small ponds, etc.), land geological sources, and oceanic sources (Saunois et al., 2020). Among them, wetland methane emissions are the largest natural source of global methane (Saunois et al., 2020) and have been found to play an important role in its interannual variation (Bousquet et al., 2006). Lakes are the second largest source after wetlands among all inland water bodies (Kyzivat et al., 2022).

Western Siberia is one of the regions releasing large amounts of methane to the atmosphere (Saunois et al., 2020). The regions dominated by large wetlands and open water bodies make them significant methane sources (Schneider et al., 2009). Western Siberia has the largest wetland area in the world, accounting for approximately

27% of the total area (Peregon et al., 2009). This makes Western Siberia the largest high-latitude wetland system experiencing warming conditions (Solomon et al., 2007). These large wetlands contain 40% peat deposits over the world (Walter, 1977), containing significant organic carbon (about 70 Pg C), and partly beneath permafrost (Sheng et al., 2004; Smith et al., 2004). The permafrost in the region is very temperature sensitive and has been thawing over the past few decades (Romanovsky et al., 2010). In a warming climate, large amounts of soil carbon deposited in permafrost regions may be released, leading to carbon degradation and the release of methane into the atmosphere (Schuur et al., 2015). Apart from extensive wetlands, this region is also characterized by large areas of aquatic ecosystems like lakes (~0.081 M km^2, Peregon et al., 2009). Driven by carbon input from surrounding terrestrial ecosystems, lake sediments generate methane through anaerobic decomposition and are eventually released into the atmosphere (Kling et al., 1992). The abundant small wetland lakes in this region can emit large amounts of methane and significantly contribute to the regional methane budget (Repo et al., 2007). As such, Western Siberia plays a crucial role in the global carbon cycle as a major natural source of atmospheric methane, and the quantification of methane emissions over the region needs to consider both wetlands and aquatic ecosystems.

The importance of Western Siberian wetlands in the global carbon cycle is indisputable, but the estimates of methane emissions from the region remain largely uncertain, ranging from 2.42 to 11.19 Tg CH_4 yr^{-1} based on different models (Bohn et al., 2015). Weak constraints on estimates of wetland and lake areas over high latitudes (e.g., Western Siberia) constitute a major uncertainty in estimating methane emissions over these regions (Melton et al., 2013; Petrescu et al., 2010). The uncertainties could originate from two sources: (a) methane emissions from wetlands and aquatic ecosystems were not both considered and quantified separately by using the suitable areal datasets; (b) the temporal dynamics of wetland and aquatic ecosystem areas were not well captured. For the first aspect, wetlands and lakes are both important sources of methane. Although many previous efforts have been made to quantify methane emissions from this region, they are limited to either wetland emissions (Bohn et al., 2015; Makushev et al., 2016) or lake emissions (Repo et al., 2007) alone. Therefore, it is important to quantify both wetland and lake areas for better estimation of methane emissions across the landscape. For the second aspect, driven by the dynamics of glaciers, seasonal snow, soil melting and freezing, the landscape over the region has complex terrestrial and aquatic ecosystems (Hinzman et al., 2005). Due to the presence of large areas of temperature-sensitive permafrost in the region, we need to apply dynamic datasets that well capture the temporal dynamics of wetland and lake areal changes into our model simulations. Wetland Area and Dynamics for Methane Modeling (WAD2M) data, recently developed by fusing multi-source surface inundation information as time series of wetland fractions, can be used as dynamic input for wetland simulations. Another inundation extent data set recently derived from the L-band Soil Moisture Active Passive (SMAP) satellite, can be used to support the methane study as the dynamic input for aquatic system simulations. The two dynamic datasets are expected to improve the quantification of methane emissions over this methane emission hot-spot region.

The innovative aspect of this paper is to exploit the recent advances in process-based models and observations from remote sensing technology. These allow us to correctly capture the dynamic changes in inundation extents of total inland water systems (i.e., wetlands and aquatic ecosystems), thus improving the methane quantification over the region from the two aspects discussed above. The innovations are implemented by applying two process-based biogeochemical models to quantify methane emissions over the region—one for wetlands and another for aquatic ecosystems. Another novel contribution of this paper lies in the usage of multi-source datasets as the inputs for the models. To investigate how different wetland areas and surface water areas affect methane emissions from these ecosystems, we used two wetland areas including one static data (Matthews & Fung, 1987) and one dynamic data (WAD2M, Zhang et al., 2021a, 2021b) for methane emissions from land, and three surface water/lake data including two static data (Messager et al., 2016; Pekel et al., 2016a) and one dynamic data from SMAP (Du et al., 2018). We combined these datasets to create four simulations for the two process-based models. With these simulations, we evaluated the influence of the variation of inundation area data on methane fluxes in both land and aquatic ecosystems over the region.

2. Methods

2.1. Study Region

Western Siberia is a geological region in Russia. It is located between the Ural Mountains to the west and the Yenisei River to the east and is bounded by the Arctic Ocean to the north and by the Altai Mountains and the

grasslands of the Eurasian Steppe to the south. In this study, we select the study region covering ~2.9 M km^2 within 62°–89°E and 53°–73°N (Figure S1 in Supporting Information S1). Nearly 80% of Western Siberia is in the Western Siberia Plain, which is one of the largest continuous plain areas in the world. Vegetation in the study region mainly includes treeless tundra (north of 66°N), taiga forest belt containing northern taiga, central taiga, and southern taiga (between 55° and 66°N), and the grasslands of the steppe (south of 55°N) (Bohn et al., 2015).

Over the study regions, except for the occasional low hills and ridges, most of them are flat plains with excess water supplies and poor drainage, thus providing favorable conditions for the formation of wetlands (Terentieva et al., 2016). These wetlands are mainly distributed in coniferous forests and tundra (Sheng et al., 2004). In addition, throughout the whole region, permanent water bodies, including lakes with an area of more than 100 km^2 to ponds with an area of less than 0.1 km^2, together with wetlands constitute the inland water system as the larger natural sources of methane emissions (Eppinga et al., 2008; Repo et al., 2007).

2.2. Model Description

2.2.1. Terrestrial Ecosystem Model (TEM)

The Terrestrial Ecosystem Model (TEM) is a process-based biogeochemical model that couples carbon, nitrogen, hydrological, and heat terrestrial processes to estimate soil thermal, soil moisture, water table depth, permafrost dynamics, as well as carbon (C) and nitrogen (N) fluxes and pool sizes at daily and monthly time steps over site level and regional scales (Zhuang et al., 2001, 2002, 2004, 2007, 2013; Melillo et al., 1993). An incorporated methane dynamics model (MDM) was developed for TEM that explicitly considers the CH_4 production (methanogenesis) process in the saturated zone, the CH_4 oxidation (methanotrophy) process in the unsaturated zone, and the CH_4 transportation from soil to the atmosphere with the effects of change in atmospheric CH_4 concentration (Zhuang et al., 2004, 2013). The net CH_4 flux between the atmosphere and soil, which is the total fluxes at the soil/water-atmosphere boundary, is determined by the relative rates of CH_4 production and oxidation within the soil profile and different CH_4 transport pathways at the soil surface. There are three pathways of methane transport between soil and the atmosphere in TEM: diffusion, plant-aided emissions, and ebullition. For uplands, diffusion is the only way that methane is transported from the atmosphere into soils, which is simulated as methane consumption. For wetlands, we consider all these three pathways and add them together as the methane emissions from wetlands. The MDM was coupled with other TEM modules: the soil thermal module (STM) to simulate the permafrost dynamics of permafrost and non-permafrost soils, the hydrological module (HM) to estimate the water movements like soil moisture dynamics and water table depth in both wetlands and uplands, and the Core C and N Dynamics Module (CNDM) to estimate the dynamics of C and N in the terrestrial biosphere using spatially explicit data about climate, vegetation, and soils. In this way, the MDM will receive information on soil temperature from STM, information on soil moisture and water table depth from HM, and carbon and vegetation characteristics from CNDM to quantify methane emissions. The version of TEM incorporated with the MDM module has been used to quantify the methane emissions in northern high-latitude regions (Zhu et al., 2014) and extrapolated into a global scale (Zhuang et al., 2013). Recently, this model was updated by considering various and more accurate wetland types and the effects of the standing water above the soil surface to establish the current TEM-MDM version with a finer time step (Liu et al., 2020). The analyses in this study are based on the latest version of the TEM-MDM model. To drive TEM-MDM, we use net primary production simulated from the Terrestrial Ecosystem Model 5.0 (TEM5).

2.2.2. Arctic Lake Biogeochemistry Model (ALBM)

The Arctic Lake Biogeochemistry Model (ALBM) is a one-dimensional process-based lake biogeochemical model that was developed to simulate the carbon and thermal dynamics of aquatic ecosystems. It was originally designed to model the processes of methane production, oxidation, and transportation from Arctic lakes (Tan and Zhuang, 2015a, 2015b; Tan et al., 2015) and then was upgraded to quantify spatiotemporal variability of the carbon dynamics in pan-Arctic lakes including CO_2 flux and phytoplankton primary production (Tan et al., 2017), and has been applied to represent the physical and biogeochemical processes of lakes in boreal regions (Guo et al., 2020; Guseva et al., 2020) and temperate regions (Guseva et al., 2020; Tan et al., 2018). Since ALBM includes the essential processes like the thawing and freezing cycles of sediments in thermokarst lakes, mobilization and mineralization of labile organic carbon in sediments of Yedoma lakes, and the representation of organic carbon induced by thermokarst activities, it is suitable to quantify methane emissions from lakes over

Table 1
Wetland and Aquatic Ecosystem Areal Data Sets Used in This Study

	Data sets	Type	Time period	Reference
Wetland	MF	Static	NA	Matthews and Fung (1987)
	WAD2M	Dynamic	2000–2020	Zhang et al. (2021a, 2021b)
Aquatic	GSW	Static	NA	Pekel et al. (2016b)
	HydroLAKES	Static	NA	Messager et al. (2016)
	SMAP	Dynamic	2016–2021	Du et al. (2018)

Western Siberia. The framework of ALBM for methane quantification incorporates several coupled modules, including a water thermal model (WTM), a sediment thermal model (STM), a gas transport model (GTM), a sediment gas model (SGM), and a bubble transport model (BTM), to consider for radiative transfer, the thermal circulation between water and sediment, the water/sediment biogeochemistry dynamics, and the gas transportation via diffusion and ebullition, respectively (Tan et al., 2015). In the model, the methane production rate in sediments and the methane oxidation rate are calculated. Methane concentrations in sediments and water columns are computed based on the methane production and oxidation rate. Finally, the methane fluxes transported to the atmosphere from water are modeled. Detailed information about ALBM can be found in previous studies (Tan et al., 2015, 2017).

2.3. Data Collection

2.3.1. Data Preparation for TEM

To obtain spatially and temporally explicit estimates of methane consumption and emission from land, we run TEM-MDM driven by one static and one dynamic wetland areal datasets (see Table 1). The widely used static wetland map from Matthews and Fung (1987) (MF for short) represents the global database of the fractional distribution of wetlands. For the dynamic wetland inundation, we use WAD2M Version 2.0 data. WAD2M was developed to reconcile the multi-model deviations of large-scale methane estimations by combining a surface inundation time series from remote sensing and a series of static datasets that distinguish different types of inundation extent (Zhang et al., 2021a, 2021b). Compared to WAD2M Version 1.0, WAD2M Version 2.0 uses the same monthly SWAMPS version 3.2 (Jensen & Mcdonald, 2019) and data processing approach but includes several updates on the static inventories applied in WAD2M. WAD2M purposely removes inundated areas so that WAD2M is supposed to represent non-inundated wetlands. Version 1.0 used the Landsat Global Surface Water Explorer (GSW) data set (Pekel et al., 2016a) to remove inland-water areas, defined as lakes, ponds, and rivers. In Version 2.0, this was replaced by other two datasets to remove inland water: one is Global River Width from Landsat (GRWL) Database (Allen & Pavelsky, 2018), which is a data set based on 30 m Landsat images describing the river width globally; another one is HydroLAKES (Messager et al., 2016), which is a global database of lakes with a surface area of at least 0.1 km^2. Within these updates, the WAD2M version 2.0 data set was developed at a spatial resolution of 0.25° × 0.25° and at a monthly time step over the 2000–2020 period.

To drive TEM-MDM, we also use spatially explicit data of climate, land cover, soil texture, soil-water pH, leaf area index (LAI), and net primary production (NPP) from various sources at a spatial resolution of 0.5° × 0.5°. The static datasets include potential natural vegetation types, cultivation type, soil texture, and soil water pH used to assign specific values for each grid cell (Zhuang et al., 2004). The dynamic inputs to drive TEM-MDM include climate, LAI, and NPP. For the climate forcing data, we used the 20CRv3-ERA5 data set (ERA5 is the fifth-generation reanalysis of ECMWF (European Centre for Medium-Range Weather Forecasts)), a global climate data set with a resolution of 0.5° × 0.5° at daily time step from the Inter-Sectoral Impact Model Intercomparison Project (ISIMIP) (Lange et al., 2022). For TEM-MDM simulations, we used climate data including precipitation (unit: mm), surface downwelling shortwave radiation (unit: W/m^2), near-surface air temperature (unit: deg C), and near-surface relative humidity (%), where air temperature and relative humidity were used to calculate the vapor pressure (unit: hPa) as another input. LAI data are obtained from ERA5 (specifically, ERA5 hourly data on single levels from 1940 to present, Hersbach et al., 2023) at a resolution of 0.25° × 0.25° at the hourly time step. We then convert LAI from ERA5 into a resolution of 0.5° × 0.5° at the monthly time step as an input for TEM-MDM. Monthly NPP was derived from TEM5 with a resolution of 0.5° × 0.5°.

2.3.2. Data Preparation for ALBM

For simulations of methane emissions from aquatic ecosystems, we use two static and one dynamic aquatic areal datasets to drive ALBM (see Table 1). One static input is the water occurrence map at 30-m resolution from GSW, which indicates the frequency with which water appears on the surface between 1984 and 2020 (Pekel et al., 2016b). As WAD2M did (Zhang et al., 2021a, 2021b), we defined those covered by open water for more than half of the months over the time period from GSW as the aquatic ecosystems. Another static input is HydroLAKES, which is a global lake data set consisting of 1.4 million individual lakes with a surface area of at least 0.1 km^2 (Messager et al., 2016). The dynamic input is a surface water inundation developed using brightness temperature data from the L-band SMAP satellite (Du et al., 2018). We derived the inundated water fraction (f_w) from the SMAP data and used it as the aquatic component of the CH_4 modeling over inundated surfaces. Specifically, f_w for each pixel was derived by:

$$f_w = 1 - \frac{r_{\text{obs}} - r_{\text{water}}}{r_{\text{land}} - r_{\text{water}}}, \text{where } r = \frac{T_{\text{BH}}}{T_{\text{BV}}} \quad (1)$$

where r_{obs} is the polarimetric ratio of the observation at a resolution of 36 km, r_{water} and r_{land} indicating the polarization ratio of a 36 km pixel with 100% water and 100% land, respectively, and T_{BH} and T_{BV} are the horizontal polarization and vertical polarization brightness temperature, respectively (Kim et al., 2017). The merits of the SMAP highly frequent temporal revisit (3 days or less) and L-band being able to penetrate vegetation and clouds to detect the underlying water (Melack et al., 2004) makes it an ideal data set mapping inundation when prevalent clouds and tall plants limit the capabilities of the optical remote sensing (such as GSW).

To drive ALBM, we used climate data from the same source as for TEM-MDM. The model forcing data include relative humidity, precipitation, air pressure, downwelling longwave radiation, downwelling shortwave radiation, wind speed, air temperature, and snowfall. The lake information, containing longitude, latitude, depth, and elevation, is obtained from HydroLAKES.

2.4. Model Simulations

We ran both TEM-MDM and ALBM pixel by pixel within the study period. All data are first re-gridded into the same spatial resolution (0.5° × 0.5°) as TEM outputs. Each grid cell is separated into up to three components: upland, wetland, and aquatic system based on the areal datasets described in Section 2.3. For uplands, we assume there is only methane consumption occurs. For wetlands, the water table depth is first simulated to determine the saturated soil zone and unsaturated soil zone—below the water table is the saturated zone, and above the water table is the unsaturated zone. In the unsaturated zone, the soil moisture is also simulated for the methane oxidation process. Methane is produced in the saturated zone and oxidized in the unsaturated zone. The methane consumption from uplands and emissions from wetlands are simulated within TEM-MDM and then are added together as the total emission from land (the positive direction is from soil surface to the atmosphere). For aquatic systems, we estimate methane emissions by adding emissions via diffusion and ebullition and these are simulated within ALBM. Finally, we aggregated emissions from land and aquatic ecosystems as the total methane flux emitted from each pixel (F_{CH_4}, Tg CH_4/year), which can be expressed as:

$$F_{\text{CH}_4} = \left(C_{\text{CH}_4} \times \text{pct}_{\text{up}} \times S + E_{\text{CH}_4\_\text{wet}} \times \text{pct}_{\text{wet}} \times S\right) + E_{\text{CH}_4\_\text{aq}} \times \text{pct}_{\text{aq}} \times S, \text{where } \text{pct}_{\text{up}} + \text{pct}_{\text{wet}} + \text{pct}_{\text{aq}} = 1 \quad (2)$$

where C_{CH_4} is methane consumption per unit area from upland (Tg CH_4/year/km^2), $E_{\text{CH}_4\_\text{wet}}$ is methane emissions per unit area from wetland (Tg CH_4/year/km^2), $E_{\text{CH}_4\_aq}$ is methane emissions per unit area from aquatic ecosystem (Tg CH_4/year/km^2), S is the pixel area (km^2), and pct_{up}, pct_{wet}, and pct_{aq} are the percentage of upland area, wetland area, and aquatic area for each pixel, respectively. In this way, on the right side of Equation 2, the sum of the first two terms is the methane emissions from land and the last term is the methane emissions from aquatic ecosystems.

There are four combinations of datasets to calculate the total methane emissions: "MF + GSW" (2000–2021), "MF + HydroLAKES" (2000–2021), "MF + SMAP" (2016–2021), and "WAD2M + HydroLAKES" (2000–2020). The reason for only using HydroLAKES as the aquatic part to combine with WAD2M as the wetland part is that WAD2M (version 2.0) exactly uses HydroLAKES as open water bodies to be removed from wetlands. Therefore, combining HydroLAKES with WAD2M can get methane emission from both land and aquatic ecosystems at the

landscape scale. For each set of simulations, we first specified the percentage of upland area, wetland area, and aquatic area within each pixel, respectively, then we multiply them by methane fluxes estimated from models to obtain the corresponding methane fluxes, as shown in Equation 2.

For wetland simulations using TEM-MDM, we first ran TEM5 over the same period to get the monthly NPP and then feed it into TEM-MDM as one of the inputs to get methane emissions. Parameters for TEM-MDM simulations are adopted from Liu et al. (2020). For lake simulations using ALBM, we first categorize all lakes over the study region into four classes based on their permafrost thawing type and the locations: temperate lakes (temperate), non-thermo boreal lakes (boreal), non-yedoma thermokarst lakes (thermokarst), and yedoma thermokarst lakes (yedoma). Among them, yedoma and thermokarst lakes are classified based on the circum-polar Yedoma map (Jens et al., 2022) and Arctic Circumpolar Distribution and Soil Carbon of Thermokarst Landscapes (Olefeldt et al., 2016). As for the rest of the lakes, the lakes above 60°N are classified as boreal lakes, and below 60°N are classified as temperate lakes. In this way, 63,398 lakes were simulated in total over the study region, including 13,895 temperate lakes, 1,877 non-thermo-boreal lakes, 45,528 non-yedoma-thermokarst lakes, and 2,098 yedoma lakes. We used different parameter sets derived from calibration for simulations of different types of lakes (Guo et al., 2021). For all simulations, we first ran a spin-up period of 40 years with ALBM and then get the model outputs over the study period.

In addition, due to the temporary hold of the SMAP instruments, there is no valid surface water inundation from 06/22/2019 to 07/22/2019 in the SMAP data set. These summer months are the peak periods of methane release, and neglecting the periods significantly underestimates the rate from 2019. As one way of estimating the missing values, we utilize the data from other years (i.e., 2016, 2017, 2018, 2020, and 2021) for the same dates. Since SMAP data are both used for ALBM for aquatic simulation and for TEM to get non-aquatic fraction and then determine wetland and upland fraction, we perform this gap-filling process for SMAP for both TEM and ALBM simulations. Specifically, for TEM simulations, we use the average value of the inundation of the same period in the other 5 years as the filling of these missing data in 2019. For ALBM simulations, we first calculate the ratios of the sum of the data for the whole year to the sum of the data for the whole year except 22 June to 22 July from the other 5 years. Then we use the average of the five ratios to recompute the value in 2019 as the gap-filled value for SMAP.

3. Results

3.1. Wetlands and Aquatic Ecosystems Areal Dynamics

We first compared the areas among different wetland and aquatic ecosystem data discussed in Section 2.3. In Figure 1, the black dashed line is the estimation of the total wetland area over Western Siberia based on a regional wetland typology map, which is 0.685 M km^2 (Peregon et al., 2009). In that study, the areal fractions of landscapes consisting of 20 mosaic vegetation types on the wetland typology map were explicitly estimated for each climate region over the study area (Peregon et al., 2009). We will use this as a baseline for the maximum area of wetlands and aquatic ecosystems. Compared to this baseline value, the wetland extent from MF is slightly larger, which is 0.699 M km^2. For WAD2M, the annual peak values of inundation extent are smaller than the baseline value. The reason is that the baseline contains both wetland and lake areas while WAD2M removed areas being defined as open water bodies. By adding the lake area removed from WAD2M (i.e., HydroLAKES) to the WAD2M time series, the annual peak values are close to the baseline. As for the three aquatic ecosystem datasets, HydroLAKES shows smaller aquatic areas compared to GSW and annual peak values of SMAP. For the two dynamic datasets, both WAD2M and SMAP show larger wetlands and open water areas around late spring and early summer (peaks around June) and reach their minimum during winter because most landscapes are frozen at that time. The difference is that there are still wetland areas during winter estimated by WAD2M while the water inundations derived from SMAP are nearly zero during that time.

3.2. Land Methane Emissions

We quantify methane consumption from upland and methane emission from wetlands over Western Siberia using TEM-MDM. We also add them together to obtain the total methane emissions from land. We evaluated annual methane outputs (mean value ± one standard deviation across corresponding temporal coverage) with different combinations of datasets (Table 1). As for methane consumption from uplands (Figure 2a), compared to using MF, using WAD2M shows slightly smaller estimates. Among the three simulations using MF, using

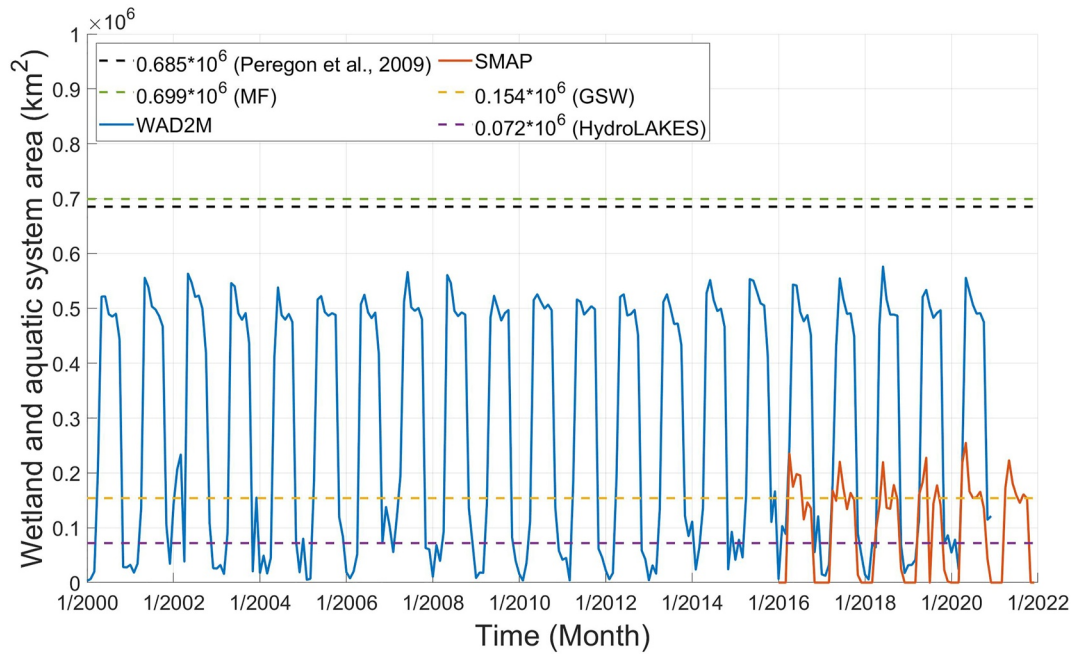

Figure 1. Monthly wetland and open water areas over the Western Siberian region based on different datasets from 2000 to 2021. The dashed lines are static data, and the solid curves are dynamic data.

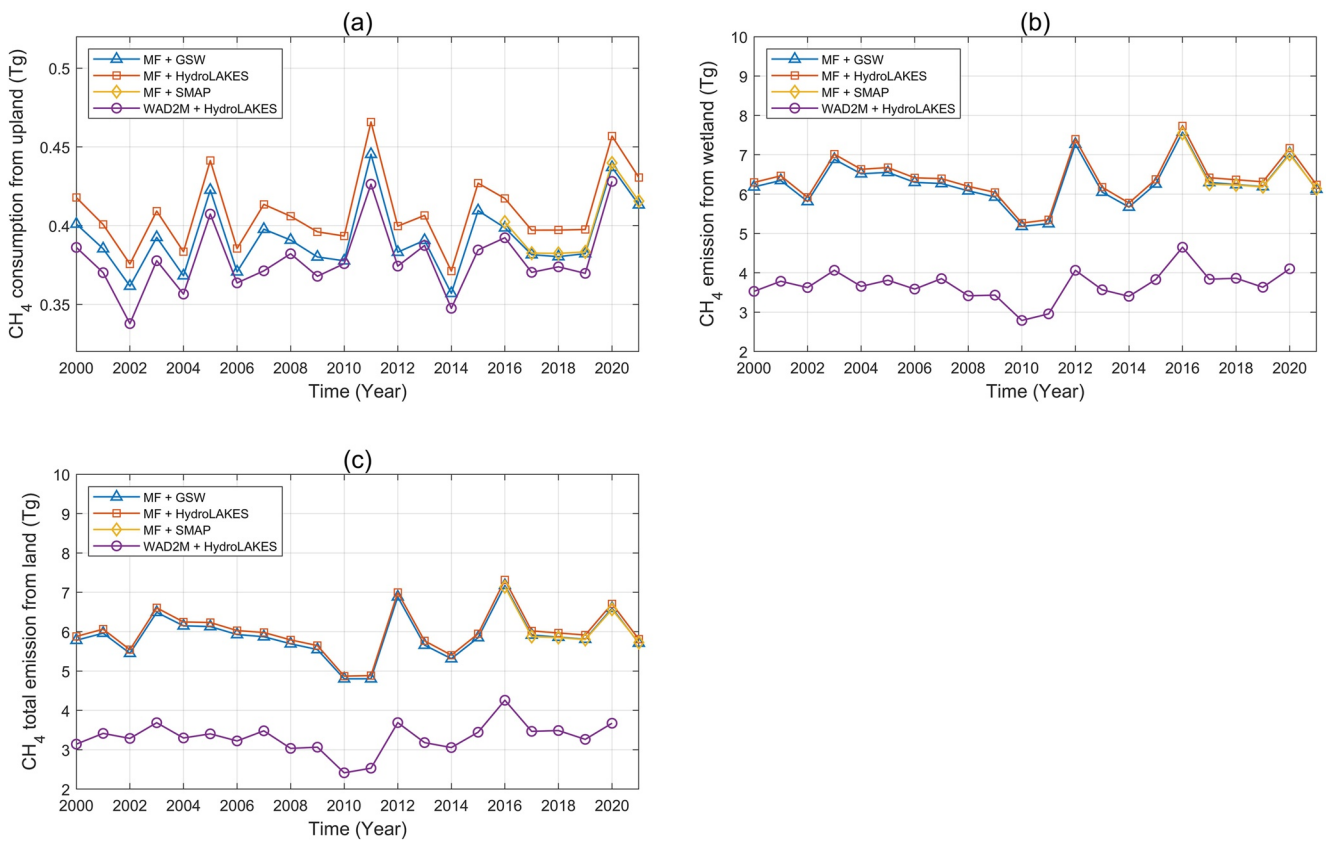

Figure 2. Annual (a) methane consumption from upland, (b) methane emission from wetlands, and (c) total methane emission from land over the Western Siberia region from 2000 to 2021.

Table 2
Methane Emissions (Tg CH_4 Yr^{-1}) From Land, Aquatic Ecosystem, and Both Over Different Time Periods ("Hydro" Is Short for "HydroLAKES" in This Table)

	Data sets	2016–2020	2016–2021	2000–2020
Land	MF + GSW	6.27 ± 0.60	6.18 ± 0.58	5.89 ± 0.58
	MF + Hydro	6.39 ± 0.61	6.29 ± 0.60	5.99 ± 0.59
	MF + SMAP	6.25 ± 0.59	6.16 ± 0.57	NA
	WAD2M + Hydro	3.63 ± 0.38	NA	3.31 ± 0.39
Aquatic	GSW	1.95 ± 0.21	1.95 ± 0.19	1.92 ± 0.15
	Hydro	1.17 ± 0.10	1.17 ± 0.09	1.15 ± 0.08
	SMAP	2.04 ± 0.60	2.01 ± 0.28	NA
Land and Aquatic	MF + GSW	8.22 ± 0.76	8.13 ± 0.71	7.80 ± 0.66
	MF + Hydro	7.56 ± 0.68	7.46 ± 0.65	7.14 ± 0.63
	MF + SMAP	8.29 ± 0.81	8.17 ± 0.78	NA
	WAD2M + Hydro	4.80 ± 0.43	NA	4.46 ± 0.62

HydroLAKES shows the largest estimations, and using GSW and using SMAP are close to each other. As for methane emissions from wetlands (Figure 2b), estimations using WAD2M are also smaller than the other three using MF. Among the three simulations using MF, using HydroLAKES shows the largest emission and the estimation using GSW is close to that using SMAP, which is like the results of methane consumption. Considering both methane consumption from upland and methane emissions from wetlands (Figure 2c), the total methane emissions from land of "MF + HydroLAKES", "MF + GSW", "MF + SMAP", and "WAD2M + HydroLAKES" is 6.39 ± 0.61, 6.27 ± 0.60, 6.25 ± 0.59, and 3.63 ± 0.38 Tg CH_4 yr^{-1} from 2016 to 2020, in descending order (see Table 2). In addition, methane emissions from land range from 6.16 ± 0.57 to 6.29 ± 0.60 Tg CH_4 yr^{-1} over 2016 to 2021 among the three simulations using MF, and range from 3.31 ± 0.39 to 5.99 ± 0.59 Tg CH_4 yr^{-1} over 2000 to 2020 among the three simulations without SMAP over the region (Table 2). The temporal trends of methane consumption from upland, emissions from wetlands, and total emissions from land are roughly the same within the study period.

3.3. Aquatic Ecosystem Methane Emissions

We quantify methane emissions from aquatic ecosystems over the region using ALBM. Like the land part, we evaluated annual methane emissions using surface areas from different aquatic datasets. In Figure 3, methane emissions from aquatic ecosystems using HydroLAKES are the smallest among the three datasets, which is 1.17 ± 0.10 Tg CH_4 yr^{-1} from 2016 to 2020 (see Table 2). The reason is that HydroLAKES only contains lakes with a surface area of at least 0.1 km^2. Therefore, it will underestimate the total area of aquatic ecosystems over the study regions, thus underestimating the methane emissions from them. Unlike HydroLAKES, both GSW and SMAP can detect open water bodies with a surface area of less than 0.1 km^2. Therefore, they show larger methane emissions at 1.95 ± 0.21 and 2.04 ± 0.60 Tg CH_4 yr^{-1} from 2016 to 2020, respectively (see Table 2). Since SMAP has the L-band ability to penetrate vegetation and cloud to detect water beneath dense canopies (Du et al., 2018; Melack et al., 2004), it can estimate more methane emissions from aquatic ecosystems. There are little differences in methane emissions from aquatic ecosystems from the same data set over different study periods (see Table 2).

3.4. Methane Emissions Across the Landscape

Combining methane emissions from Figures 2c and 3, we get the annual total methane emissions from both land and aquatic ecosystems over Western Siberia (Figure 4). The total methane emissions of "MF + SMAP", "MF + GSW", "MF + HydroLAKES", and "WAD2M + HydroLAKES" is 8.29 ± 0.81, 8.22 ± 0.76, 7.56 ± 0.68, and 4.80 ± 0.43 Tg CH_4 yr^{-1} from 2016 to 2020, respectively, in a descending order (see Table 2). For all four simulations, the highest values of annual total methane emissions appear in 2016, and the lowest values of annual total methane emissions appear in 2010 (except for "MF + SMAP" since no data was available before 2016). In addition, the total methane emissions over the region range from 7.46 ± 0.65 to 8.17 ± 0.78 Tg CH_4 yr^{-1} over 2016 to 2021 with the three simulations using MF and 4.46 ± 0.62 to 7.80 ± 0.66 Tg CH_4 yr^{-1} over 2000 to

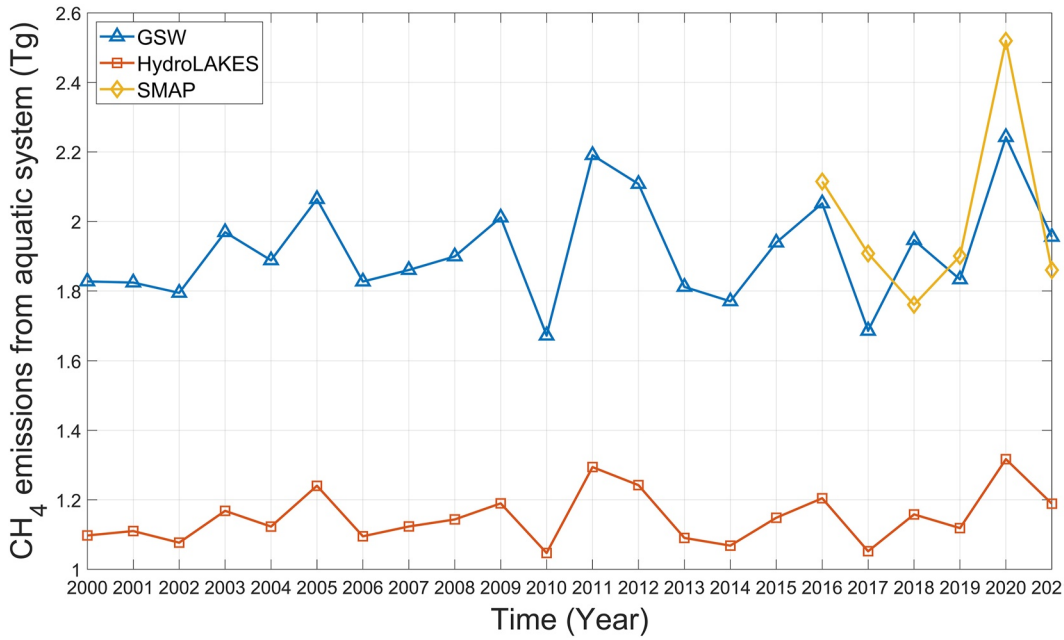

Figure 3. Annual methane emissions from aquatic ecosystems over the Western Siberia region from 2000 to 2021.

2020 with the three simulations without SMAP. For estimates of total methane emissions for each time range, "MF + SMAP" is the largest and "WAD2M + HydroLAKES" is the smallest as long as they are available.

The spatial distributions of the annual mean total methane emissions from both land and aquatic ecosystems over the region are shown in Figure 5. In this figure, we used the largest time range available for each combination of datasets. For the four simulations, areas with large methane emissions are all concentrated between 55°N and 65°N, especially in 67°–73°E and 57°–60°N, which are mainly boreal forests and non-forested boreal wetlands.

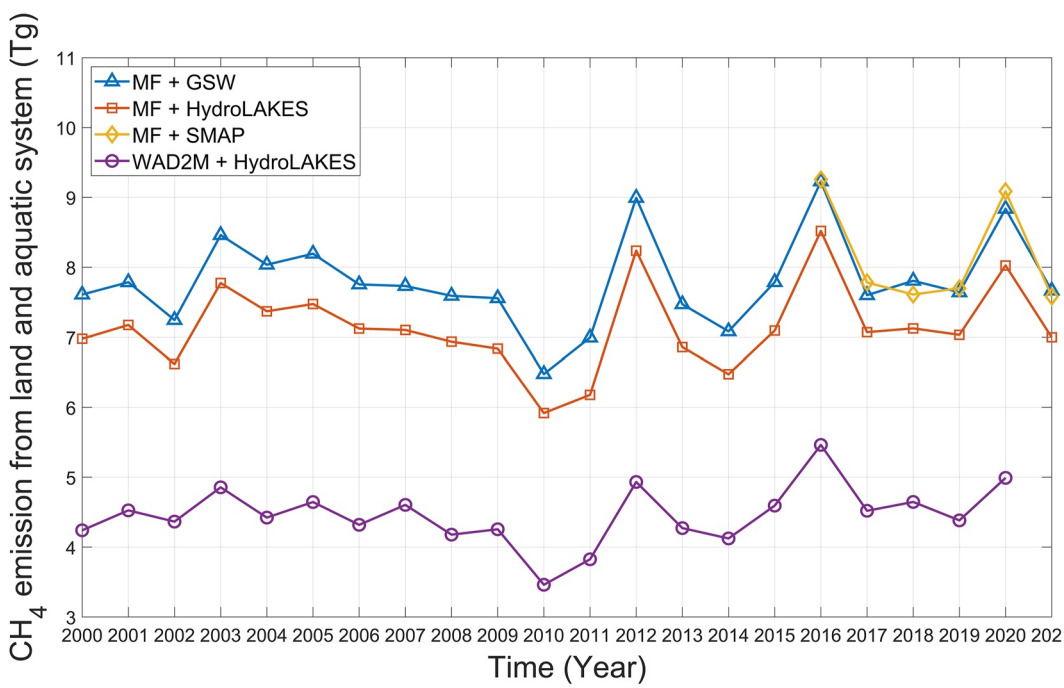

Figure 4. Annual methane emissions from both land and aquatic ecosystems over the Western Siberia region from 2000 to 2021.

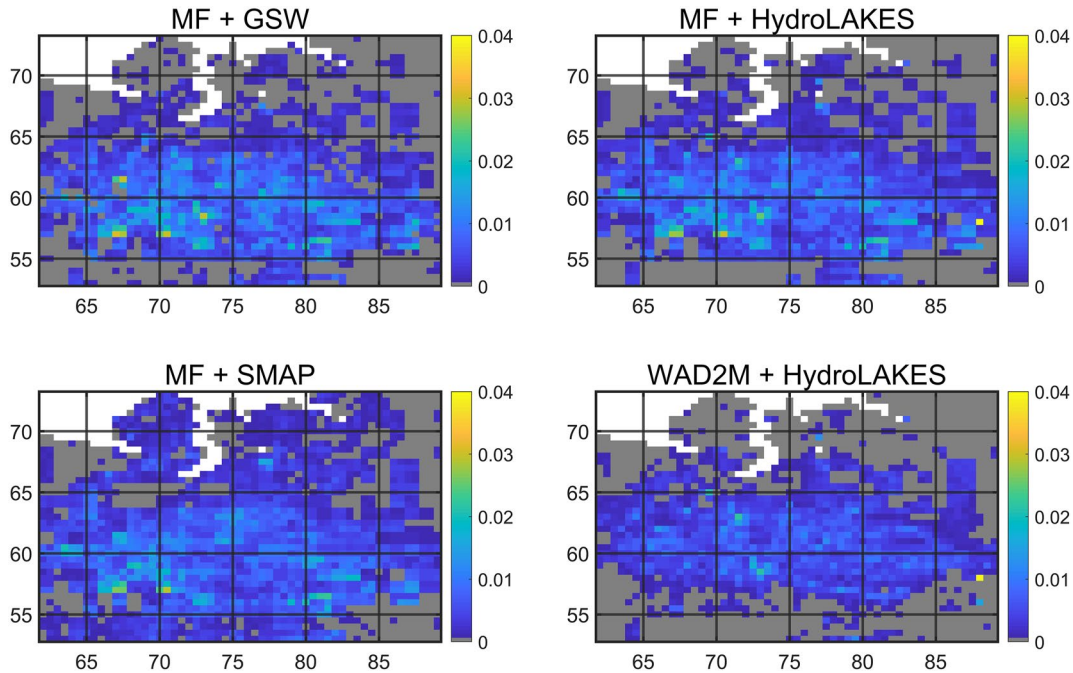

Figure 5. Spatial distribution of annual mean total methane emissions (Tg CH_4 yr^{-1}) from both land and aquatic ecosystems over the Western Siberia region. The dark gray are the regions where methane emissions are zero.

On the other hand, there are large amounts of areas with zero methane emissions concentrated in regions below 55°N and above 65°N. Among the four simulations, the regions with zero methane emissions are the largest for "WAD2M + HydroLAKES". In addition, other regions of "WAD2M + HydroLAKES" show smaller estimates than the other three simulations. Compared to other simulations, "MF + SMAP" shows the least regions without methane emissions, especially in the Yamal Peninsula where is mainly wet tundra, and in the southwest region where are mainly tall grasslands. Since the other three simulations do not include SMAP data, this indicates that only SMAP has the ability to detect open water bodies with small surface areas under the dense vegetation, and thus can estimate the methane emissions from aquatic ecosystems over these regions.

4. Discussion

4.1. Annual and Monthly Methane Emissions Comparison

As for the annual total methane emissions from both land and aquatic ecosystems (Figure 4), the magnitude of "WAD2M + HydroLAKES" is smaller than the other three simulations, which might overestimate the total methane emissions since MF does not remove the open water bodies like WAD2M. As for the three simulations using MF, "MF + HydroLAKES" estimates the least annual methane emissions. The reason is that HydroLAKES only contains lakes and reservoirs with surface area larger than 0.1 km^2 (Messager et al., 2016), which means that "MF + HydroLAKES" does not include methane emissions from small lakes. However, there are larger amounts of small lakes and ponds in Western Siberia (Repo et al., 2007). Furthermore, small lakes and ponds have been found to have large methane emissions (Holgerson & Raymond, 2016; Matthews et al., 2020). Therefore, using HydroLAKES would underestimate methane emissions from aquatic ecosystems. Compared to HydroLAKES, GSW includes any open water bodies larger than 30 m × 30 m (Pekel et al., 2016b), which means it contains methane emissions from lakes with surface area between 0.0009 and 0.1 km^2. Therefore, "MF + GSW" estimates more total methane emissions than "MF + HydroLAKES" because the former estimates more methane emissions from aquatic ecosystems. The "MF + SMAP" estimates are larger than both "MF + GSW" and "MF + HydroLAKES". Apart from the fact that SMAP can detect small lakes like GSW, its L-band ability to penetrate vegetation and clouds to detect underlying inundation (Du et al., 2018; Melack et al., 2004) can also make it estimate more methane emissions from aquatic ecosystems. In addition, since SMAP inundation is dynamic, it can more accurately reflect the dynamic changes in the area of aquatic systems, and thus obtain more accurate methane emissions.

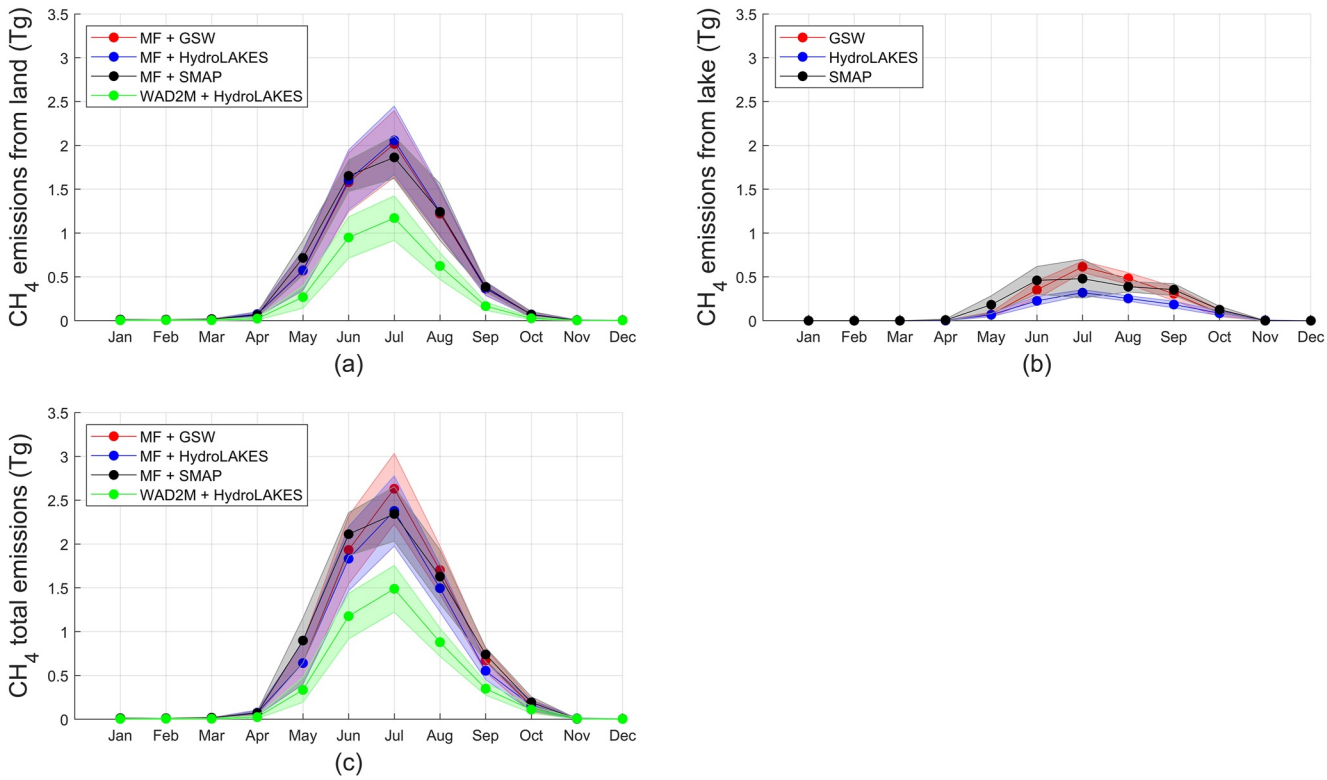

Figure 6. Monthly mean of methane emissions from (a) land; (b) aquatic ecosystems; and (c) both land and aquatic ecosystems over Western Siberia. The shading for each simulation set represents +/− one standard deviation.

Apart from the comparison of annual methane emissions among the four simulations, we also compare their monthly methane emissions (Figure 6). This monthly analysis does not include data from June and July in 2019 for "MF + SMAP" due to the missing values from SMAP in these months. The four simulations show similar monthly variability. The methane emissions are mainly concentrated in the summer season (JJA). The peak values of total methane emissions are all achieved in July, followed by June and August. There are nearly no methane emissions occurring in the winter season (DJF) when the wetlands and aquatic ecosystems are nearly all frozen. Among the four simulations of total emissions, "WAD2M + HydroLAKES" has the minimum estimates in each month. For the other three simulations, the total estimations from "MF + HydroLAKES" are the smallest in most months, and "MF + SMAP" estimates higher total methane emissions than "MF + GSW" in May, June, and September. Considering that SMAP is dynamic, this result shows that SMAP can detect more inundation areas in these months, indicating that Western Siberia could thaw faster and more extensively than the estimate from static data (i.e., GSW and HydroLAKES). The methane emissions from land and aquatic ecosystems both contribute to these higher estimations made by "MF + SMAP". In addition, by using the dynamic inundation data set (i.e., SMAP), we can estimate total methane emissions that occur in the peak month (i.e., July), which are smaller than "MF + GSW". This lower estimation is mainly due to the lower estimations from aquatic ecosystems.

Table 3
Correlations Between Monthly Total Methane Emissions and Climate Drivers ("Hydro" Is Short for "HydroLAKES" in This Table)

	Precipitation	Solar radiation	Air temperature	Vapor pressure
MF + GSW	0.71	0.72	0.85	0.95
MF + Hydro	0.70	0.74	0.85	0.94
MF + SMAP	0.75	0.77	0.87	0.92
WAD2M + Hydro	0.70	0.72	0.84	0.94
Average	0.72	0.74	0.85	0.94

4.2. Spatiotemporal Correlation Between Methane Emissions and Climate Drivers

We conduct correlation analysis between monthly time series of total methane emissions and the four climate drivers—precipitation, solar radiation, air temperature, and vapor pressure, to examine the main drivers for our simulation. Correlation analysis of the four simulation sets is conducted within their available time periods. In Table 3, all correlation sets are statistically significant with a p-value smaller than 0.01. The four simulations show the

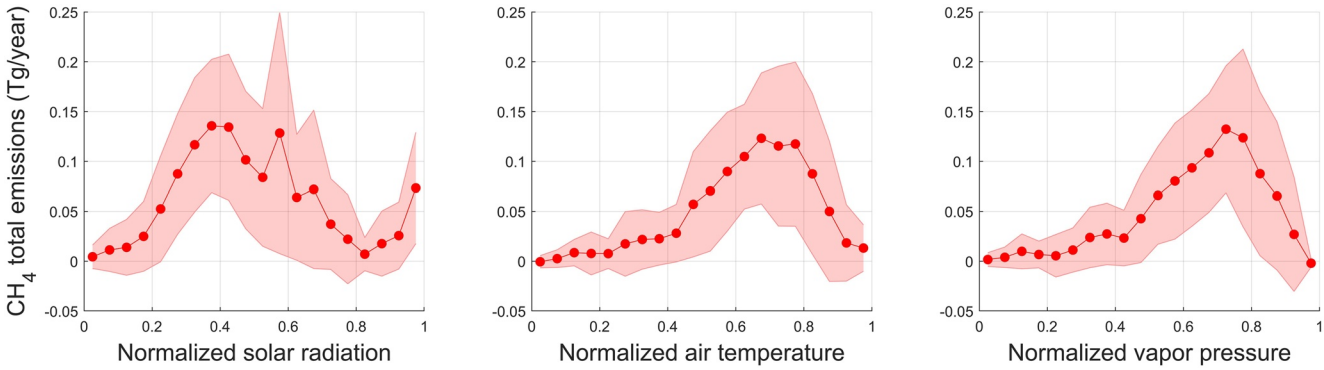

Figure 7. Relationships between the total methane emissions and the normalized mean of three climate drivers. The red shading represents +/− one standard deviation. For each subplot, each climate driver is first separated into 20 bins of equal size (i.e., 0.05 for each bin), then the mean value of averaged total methane emissions among the four simulations located in each bin is separately calculated for each climate driver.

same correlation behavior with the four climate drivers. Among the climate drivers, vapor pressure shows the highest correlation coefficient with total methane emissions, which is 0.94 on average. Vapor pressure influencing methane emissions is modeled in TEM. Specifically, higher vapor pressure will reduce evapotranspiration (ET) by limiting stomatal openness, and the reduction of ET will increase soil moisture. Water table depth will be higher, increasing the thickness of the saturated zone, and producing more methane. As a result, vapor pressure and methane production show a high correlation. The second largest is air temperature, followed by solar radiation and precipitation. Therefore, the monthly variability of total methane emissions over the region can be mainly captured by vapor pressure and air temperature.

In addition, we evaluate how the spatial distribution of the climate drivers affects the spatial distribution of total methane emissions. For each climate driver, we first get the mean values across the study period, then we normalize the temporal mean values within zero to one based on the min-max normalization (Figure S2 in Supporting Information S1). Then we check the relationships between total methane emissions and normalized mean values of climate drivers. Since the spatial distribution of precipitation is relatively uniform (see Figure S2 in Supporting Information S1), which means that it is hard to capture the spatial variability of precipitation over the region, we only check this relationship with the other three climate drivers. Figure 7 shows the spatial relationship of total methane emissions to the three climate drivers. For solar radiation, the methane emissions mainly concentrate in the middle range from about 30% to 60%. For air temperature and vapor pressure, the methane emissions are both concentrated in relatively larger regions, from about 60% to 80% of the total amounts. For both, the smallest 30% of the total area has extremely small methane emissions.

4.3. Comparison With Other Studies and Future Work

The Wetland and Wetland CH4 Intercomparison of Models Project (WETCHIMP), focused on the Western Siberian Lowland (WETCHIMP-WSL), estimating methane emissions from wetlands including small ponds or lakes but excluding rivers and large lakes based on forward models, inversions, and in situ observations (Bohn et al., 2015). The models involved in this project have different hydrological modeling approaches, soil thermal physics and biogeochemical schemes, and different ways of defining the area where methane is produced. Among these models, some of them use the Global Inundation Extent from Multi-Satellites (GIEMS; Prigent et al., 2007; Papa et al., 2010) product to prescribe dynamic wetland extent, some other models use topographic information and a distributed water table approach to predict the area producing methane, and the remaining models rely on wetland maps alone or in combination with surface water products to provide wetland information (Bohn et al., 2015). In that study, they estimated 5.34 ± 0.54 Tg CH_4 yr^{-1} based on 21 models (ranging from 2.42 to 11.19 Tg CH_4 yr^{-1}), 6.06 ± 1.22 Tg CH_4 yr^{-1} based on five inversions (ranging from 3.08 to 9.80 Tg CH_4 yr^{-1}), and 3.91 ± 1.29 Tg CH_4 yr^{-1} from in situ observations as 12-year (1993–2004) mean estimates of total methane emissions over the WSL (Bohn et al., 2015). Makushev et al. (2016) used Regional Climate Model (RegCM4) and soil properties from Community Land Model (CLM4.5) to estimate 4.34 Tg yr^{-1} methane emissions from wetland ecosystems over West Siberia from 2000 to 2013. Compared to other studies, our estimates with different wetlands and aquatic area datasets over the region are within the range of previous estimates. Unlike those studies, we explicitly quantify emissions from both land and aquatic ecosystems.

Although our estimates are based on state-of-the-art wetlands and aquatic area datasets, uncertainties and limitations of our estimation still exist. The major one is the combination of both dynamic wetland areas and dynamic aquatic ecosystem areas. In this study, we use WAD2M as the wetland area data set and combine it with HydroLAKES as the lake area data set to cover all methane emission ecosystems at the landscape scale. Although WAD2M can capture dynamic changes in wetland areas and thus provide more accurate methane emissions from wetlands, HydroLAKES is still static and only contains lakes with surface areas larger than 0.1 km^2. Therefore, it would underestimate methane emissions from lakes. SMAP is dynamic data representing aquatic ecosystem areas, but it has not been used in WAD2M to calculate wetland areas. Thus, it is a research propriety to develop dynamic wetland and upland area data based on SMAP data. The dynamic data of wetlands, uplands, and aquatic ecosystems at the landscape scale will be important to quantify methane emissions from this region.

5. Conclusions

In this study, we applied two process-based biogeochemistry models to quantify methane emissions from land and aquatic ecosystems over Western Siberia from 2000 to 2021. We compared four sets of model simulations driven by different combinations of wetland and aquatic area datasets within three different temporal coverage based on the data availability. Our results show that, for land simulations, MF estimates larger emissions than WAD2M. For lake simulations, GSW and SMAP estimate larger emissions than HydroLAKES. Considering both land and aquatic ecosystems, the total methane emissions over the region range from 4.80 ± 0.43 Tg CH_4 yr^{-1} (using WAD2M and HydroLAKES) to 8.29 ± 0.81 Tg CH_4 yr^{-1} (using MF and SMAP) from 2016 to 2020, which is the intersection period of four simulations. We also conducted the comparisons within other two time periods, and we found that total methane emissions over the region range from 7.46 ± 0.65 to 8.17 ± 0.78 Tg CH_4 yr^{-1} from 2016 to 2021 with the three simulations using MF and 4.46 ± 0.62 to 7.80 ± 0.66 Tg CH_4 yr^{-1} from 2000 to 2020 with the three simulations without SMAP. For all the simulations, the total methane emissions are most affected by vapor pressure, followed by air temperature, solar radiation, and precipitation.

Among the four simulations, "WAD2M + HydroLAKES" estimates the smallest total methane emissions because HydroLAKES is missing many small lakes which can also contribute large amounts of emissions. Instead, the treatment of SMAP inundation datasets in this study makes it a dynamic aquatic areal data set showing the ability to detect open water bodies with small surface areas. We conclude that it is important to quantify methane emissions from wetlands and aquatic ecosystems simultaneously for regional analysis. In addition, developing dynamic wetland and aquatic areal data is necessary for quantifying regional and global methane emissions.

Data Availability Statement

The codes and data for analysis in this study are available at Purdue University Research Repository: Xi, X.; Zhuang, Q.; Kim, S.; Zhang, Z. (2023). Methane emissions from land and aquatic ecosystems in Western Siberia: An analysis with methane biogeochemistry models. Purdue University Research Repository. https://doi.org/10.4231/80RV-X686.

Acknowledgments
Zhuang was funded by NASA through a subcontract from JPL 1609311. The supercomputing is provided by the Rosen Center for Advanced Computing at Purdue University.

References

Allen, G. H., & Pavelsky, T. M. (2018). Global extent of rivers and streams. *Science*, *361*(6402), 585–588. https://doi.org/10.1126/science.aat0636

Bohn, T. J., Melton, J. R., Ito, A., Kleinen, T., Spahni, R., Stocker, B. D., et al. (2015). WETCHIMP-WSL: Intercomparison of wetland methane emissions models over West Siberia. *Biogeosciences*, *12*(11), 3321–3349. https://doi.org/10.5194/bg-12-3321-2015

Bousquet, P., Ciais, P., Miller, J. B., Dlugokencky, E. J., Hauglustaine, D. A., Prigent, C., et al. (2006). Contribution of anthropogenic and natural sources to atmospheric methane variability. *Nature*, *443*(7110), 439–443. https://doi.org/10.1038/nature05132

Ciais, P., Sabine, C., Bala, G., Bopp, L., Brovkin, V., Canadell, J., et al. (2013). Carbon and other biogeochemical cycles. Climate change 2013: The physical science basis. Contribution of working Group I to the fifth assessment report of the intergovernmental panel on climate change. *Computational Geometry*, *18*, 95–123.

Du, J., Kimball, J. S., Galantowicz, J., Kim, S. B., Chan, S. K., Reichle, R., et al. (2018). Assessing global surface water inundation dynamics using combined satellite information from SMAP, AMSR2 and Landsat [Dataset]. Remote Sensing of Environment, *213*, 1–17. https://doi.org/10.1016/j.rse.2018.04.054

Eppinga, M. B., Rietkerk, M., Borren, W., Lapshina, E. D., Bleuten, W., & Wassen, M. J. (2008). Regular surface patterning of peatlands: Confronting theory with field data. *Ecosystems*, *11*(4), 520–536. https://doi.org/10.1007/s10021-008-9138-z

Guo, M., Zhuang, Q., Tan, Z., Shurpali, N., Juutinen, S., Kortelainen, P., & Martikainen, P. J. (2020). Rising methane emissions from boreal lakes due to increasing ice-free days. *Environmental Research Letters*, *15*(6), 064008. https://doi.org/10.1088/1748-9326/ab8254

Guo, M., Zhuang, Q., Yao, H., Golub, M., Leung, L. R., Pierson, D., & Tan, Z. (2021). Validation and sensitivity analysis of a 1-D lake model across global lakes. *Journal of Geophysical Research: Atmospheres*, *126*(4), e2020JD033417. https://doi.org/10.1029/2020jd033417

Guseva, S., Bleninger, T., Jöhnk, K., Polli, B. A., Tan, Z., Thiery, W., et al. (2020). Multimodel simulation of vertical gas transfer in a temperate lake. *Hydrology and Earth System Sciences*, *24*(2), 697–715. https://doi.org/10.5194/hess-24-697-2020

Hersbach, H., Bell, B., Berrisford, P., Biavati, G., Horányi, A., Muñoz Sabater, J., et al. (2023). ERA5 hourly data on single levels from 1940 to present [Dataset]. Copernicus Climate Change Service (C3S) Climate Data Store (CDS). https://doi.org/10.24381/cds.adbb2d47

Hinzman, L. D., Bettez, N. D., Bolton, W. R., Chapin, F. S., Dyurgerov, M. B., Fastie, C. L., et al. (2005). Evidence and implications of recent climate change in northern Alaska and other arctic regions. *Climatic Change*, *72*(3), 251–298. https://doi.org/10.1007/s10584-005-5352-2

Holgerson, M. A., & Raymond, P. A. (2016). Large contribution to inland water CO_2 and CH_4 emissions from very small ponds. *Nature Geoscience*, *9*(3), 222–226. https://doi.org/10.1038/ngeo2654

Jens, S., Laboor, S., Schirrmeister, L., Fedorov, A. N., Fortier, D., Froese, D. G., et al. (2022). Database of ice-rich Yedoma permafrost version 2 (IRYP v2) [Dataset]. PANGAEA. https://doi.org/10.1594/PANGAEA.940078

Jensen, K., & Mcdonald, K. (2019). Surface water microwave product series version 3: A near-real time and 25-year historical global inundated area fraction time series from active and passive microwave remote sensing. *IEEE Geoscience and Remote Sensing Letters*, *16*(9), 1402–1406. https://doi.org/10.1109/lgrs.2019.2898779

Kim, S., Brisco, B., & Poncos, V. (2017). Inundation extent monitoring with SMAP data for carbon studies. In *2017 IEEE international geoscience and remote sensing symposium (IGARSS)* (pp. 5693–5696). IEEE.

Kling, G. W., Kipphut, G. W., & Miller, M. C. (1992). The flux of CO_2 and CH_4 from lakes and rivers in arctic Alaska. *Hydrobiologia*, *240*(1–3), 23–36. https://doi.org/10.1007/bf00013449

Kyzivat, E. D., Smith, L. C., Garcia-Tigreros, F., Huang, C., Wang, C., Langhorst, T., et al. (2022). The importance of lake emergent aquatic vegetation for estimating arctic-boreal methane emissions. *Journal of Geophysical Research: Biogeosciences*, *127*(6), e2021JG006635. https://doi.org/10.1029/2021jg006635

Lange, S., Mengel, M., Treu, S., & Büchner, M. (2022). ISIMIP3a atmospheric climate input data (v1.0) [Dataset]. ISIMIP Repository. https://doi.org/10.48364/ISIMIP.982724

Liu, L., Zhuang, Q., Oh, Y., Shurpali, N. J., Kim, S., & Poulter, B. (2020). Uncertainty quantification of global net methane emissions from terrestrial ecosystems using a mechanistically based biogeochemistry model. *Journal of Geophysical Research: Biogeosciences*, *125*(6), e2019JG005428. https://doi.org/10.1029/2019jg005428

Makushev, K. M., Lagutin, A. A., Volkov, N. V., & Mordvin, E. Y. (2016). Methane emission from Western Siberia's wetland ecosystems in the first half of the XXI century. In *22nd international symposium on atmospheric and ocean optics: Atmospheric physics* (Vol. 10035, pp. 1312–1318). SPIE.

Matthews, E., & Fung, I. (1987). Methane emission from natural wetlands: Global distribution, area, and environmental characteristics of sources [Dataset]. Global Biogeochemical Cycles, *1*(1), 61–86. https://doi.org/10.1029/GB001i001p00061

Matthews, E., Johnson, M. S., Genovese, V., Du, J., & Bastviken, D. (2020). Methane emission from high latitude lakes: Methane-centric lake classification and satellite-driven annual cycle of emissions. *Scientific Reports*, *10*(1), 1–9. https://doi.org/10.1038/s41598-020-68246-1

Melack, J. M., Hess, L. L., Gastil, M., Forsberg, B. R., Hamilton, S. K., Lima, I. B., & Novo, E. M. (2004). Regionalization of methane emissions in the Amazon Basin with microwave remote sensing. *Global Change Biology*, *10*(5), 530–544. https://doi.org/10.1111/j.1365-2486.2004.00763.x

Melillo, J. M., McGuire, A. D., Kicklighter, D. W., Moore, B., Vorosmarty, C. J., & Schloss, A. L. (1993). Global climate change and terrestrial net primary production. *Nature*, *363*(6426), 234–240. https://doi.org/10.1038/363234a0

Melton, J. R., Wania, R., Hodson, E. L., Poulter, B., Ringeval, B., Spahni, R., et al. (2013). Present state of global wetland extent and wetland methane modelling: Conclusions from a model inter-comparison project (WETCHIMP). *Biogeosciences*, *10*(2), 753–788. https://doi.org/10.5194/bg-10-753-2013

Messager, M. L., Lehner, B., Grill, G., Nedeva, I., & Schmitt, O. (2016). Estimating the volume and age of water stored in global lakes using a geo-statistical approach [Dataset]. Nature Communications, *7*(1), 13603. https://doi.org/10.1038/ncomms13603

Olefeldt, D., Goswami, S., Grosse, G., Hayes, D. J., Hugelius, G., Kuhry, P., et al. (2016). Arctic circumpolar distribution and soil carbon of thermokarst landscapes, 2015 [Dataset]. ORNL DAAC. https://doi.org/10.3334/ORNLDAAC/1332

Papa, F., Prigent, C., Aires, F., Jimenez, C., Rossow, W. B., & Matthews, E. (2010). Interannual variability of surface water extent at the global scale, 1993–2004. *Journal of Geophysical Research*, *115*(D12), D12111. https://doi.org/10.1029/2009jd012674

Pekel, J.-F., Cottam, A., Gorelick, N., & Belward, A. S. (2016a). High-resolution mapping of global surface water and its long-term changes [Dataset]. Nature, *540* (7633), 418–422. https://doi.org/10.1038/nature20584

Pekel, J. F., Cottam, A., Gorelick, N., & Belward, A. S. (2016b). High-resolution mapping of global surface water and its long-term changes. *Nature*, *540*(7633), 418–422. https://doi.org/10.1038/nature20584

Peregon, A., Maksyutov, S., & Yamagata, Y. (2009). An image-based inventory of the spatial structure of West Siberian wetlands. *Environmental Research Letters*, *4*(4), 045014. https://doi.org/10.1088/1748-9326/4/4/045014

Petrescu, A. M. R., Van Beek, L. P. H., Van Huissteden, J., Prigent, C., Sachs, T., Corradi, C. A. R., et al. (2010). Modeling regional to global CH_4 emissions of boreal and arctic wetlands. *Global Biogeochemical Cycles*, *24*(4), GB4009. https://doi.org/10.1029/2009gb003610

Prigent, C., Papa, F., Aires, F., Rossow, W. B., & Matthews, E. (2007). Global inundation dynamics inferred from multiple satellite observations, 1993–2000. *Journal of Geophysical Research*, *112*(D12), D12107. https://doi.org/10.1029/2006jd007847

Repo, E., Huttunen, J. T., Naumov, A. V., Chichulin, A. V., Lapshina, E. D., Bleuten, W., & Martikainen, P. J. (2007). Release of CO_2 and CH_4 from small wetland lakes in western Siberia. *Tellus B: Chemical and Physical Meteorology*, *59*(5), 788–796. https://doi.org/10.3402/tellusb.v59i5.17058

Romanovsky, V. E., Drozdov, D. S., Oberman, N. G., Malkova, G. V., Kholodov, A. L., Marchenko, S. S., et al. (2010). Thermal state of permafrost in Russia. *Permafrost and Periglacial Processes*, *21*(2), 136–155. https://doi.org/10.1002/ppp.683

Saunois, M., Stavert, A. R., Poulter, B., Bousquet, P., Canadell, J. G., Jackson, R. B., et al. (2020). The global methane budget 2000–2017. *Earth System Science Data*, *12*(3), 1561–1623. https://doi.org/10.5194/essd-12-1561-2020

Schneider, J., Grosse, G., & Wagner, D. (2009). Land cover classification of tundra environments in the Arctic Lena Delta based on Landsat 7 ETM+ data and its application for upscaling of methane emissions. *Remote Sensing of Environment*, *113*(2), 380–391. https://doi.org/10.1016/j.rse.2008.10.013

Schuur, E. A., McGuire, A. D., Schädel, C., Grosse, G., Harden, J. W., Hayes, D. J., et al. (2015). Climate change and the permafrost carbon feedback. *Nature*, *520*(7546), 171–179. https://doi.org/10.1038/nature14338

Sheng, Y., Smith, L. C., MacDonald, G. M., Kremenetski, K. V., Frey, K. E., Velichko, A. A., et al. (2004). A high-resolution GIS-based inventory of the west Siberian peat carbon pool. *Global Biogeochemical Cycles*, *18*(3), GB3004. https://doi.org/10.1029/2003gb002190

Smith, L. C., MacDonald, G. M., Velichko, A. A., Beilman, D. W., Borisova, O. K., Frey, K. E., et al. (2004). Siberian peatlands a net carbon sink and global methane source since the early Holocene. *Science*, *303*(5656), 353–356. https://doi.org/10.1126/science.1090553

Solomon, S., Qin, D., Manning, M., Averyt, K., & Marquis, M. (Eds.) (2007)., *Climate change 2007-the physical science basis: Working group I contribution to the fourth assessment report of the IPCC* (Vol. 4). Cambridge university press.

Tan, Z., Yao, H., & Zhuang, Q. (2018). A small temperate lake in the 21st century: Dynamics of water temperature, ice phenology, dissolved oxygen, and chlorophyll a. *Water Resources Research*, *54*(7), 4681–4699. https://doi.org/10.1029/2017wr022334

Tan, Z., & Zhuang, Q. (2015a). Methane emissions from pan-Arctic lakes during the 21st century: An analysis with process-based models of lake evolution and biogeochemistry. *Journal of Geophysical Research: Biogeosciences*, *120*(12), 2641–2653. https://doi.org/10.1002/2015jg003184

Tan, Z., & Zhuang, Q. (2015b). Arctic lakes are continuous methane sources to the atmosphere under warming conditions. *Environmental Research Letters*, *10*(5), 054016. https://doi.org/10.1088/1748-9326/10/5/054016

Tan, Z., Zhuang, Q., Shurpali, N. J., Marushchak, M. E., Biasi, C., Eugster, W., & Walter Anthony, K. (2017). Modeling CO_2 emissions from Arctic lakes: Model development and site-level study. *Journal of Advances in Modeling Earth Systems*, *9*(5), 2190–2213. https://doi.org/10.1002/2017ms001028

Tan, Z., Zhuang, Q., & Walter Anthony, K. (2015). Modeling methane emissions from arctic lakes: Model development and site-level study. *Journal of Advances in Modeling Earth Systems*, *7*(2), 459–483. https://doi.org/10.1002/2014ms000344

Terentieva, I. E., Glagolev, M. V., Lapshina, E. D., Sabrekov, A. F., & Maksyutov, S. (2016). Mapping of west Siberian taiga wetland complexes using Landsat imagery: Implications for methane emissions. *Biogeosciences*, *13*(16), 4615–4626. https://doi.org/10.5194/bg-13-4615-2016

Walter, B. P., Heimann, M., & Matthews, E. (2001). Modeling modern methane emissions from natural wetlands: 1. Model description and results. *Journal of Geophysical Research*, *106*(D24), 34189–34206. https://doi.org/10.1029/2001jd900165

Walter, H. (1977). The oligotrophic peatlands of Western Siberia-the largest Peino-Helobiome in the world. *Vegetatio*, *34*(3), 167–178. https://doi.org/10.1007/bf00055213

Zhang, Z., Fluet-Chouinard, E., Jensen, K., McDonald, K., Hugelius, G., Gumbricht, T., et al. (2021a). Development of a global dataset of wetland area and Dynamics for methane modeling (WAD2M) (2.0) [Dataset]. Zenodo. https://doi.org/10.5281/zenodo.5553187

Zhang, Z., Fluet-Chouinard, E., Jensen, K., McDonald, K., Hugelius, G., Gumbricht, T., et al. (2021b). Development of the global dataset of wetland area and Dynamics for methane modeling (WAD2M). *Earth System Science Data*, *13*(5), 2001–2023. https://doi.org/10.5194/essd-13-2001-2021

Zhu, X., Zhuang, Q., Lu, X., & Song, L. (2014). Spatial scale-dependent land–atmospheric methane exchanges in the northern high latitudes from 1993 to 2004. *Biogeosciences*, *11*(7), 1693–1704. https://doi.org/10.5194/bg-11-1693-2014

Zhuang, Q., Chen, M., Xu, K., Tang, J., Saikawa, E., Lu, Y., et al. (2013). Response of global soil consumption of atmospheric methane to changes in atmospheric climate and nitrogen deposition. *Global Biogeochemical Cycles*, *27*(3), 650–663. https://doi.org/10.1002/gbc.20057

Zhuang, Q., McGuire, A. D., O'neill, K. P., Harden, J. W., Romanovsky, V. E., & Yarie, J. (2002). Modeling soil thermal and carbon dynamics of a fire chronosequence in interior Alaska. *Journal of Geophysical Research*, *107*(D1), FFR-3.

Zhuang, Q., Melillo, J. M., Kicklighter, D. W., Prinn, R. G., McGuire, A. D., Steudler, P. A., et al. (2004). Methane fluxes between terrestrial ecosystems and the atmosphere at northern high latitudes during the past century: A retrospective analysis with a process-based biogeochemistry model. *Global Biogeochemical Cycles*, *18*(3), GB3010. https://doi.org/10.1029/2004gb002239

Zhuang, Q., Melillo, J. M., McGuire, A. D., Kicklighter, D. W., Prinn, R. G., Steudler, P. A., et al. (2007). Net emissions of CH_4 and CO_2 in Alaska: Implications for the region's greenhouse gas budget. *Ecological Applications*, *17*(1), 203–212. https://doi.org/10.1890/1051-0761(2007)017[0203:neocac]2.0.co;2

Zhuang, Q., Romanovsky, V. E., & McGuire, A. D. (2001). Incorporation of a permafrost model into a large-scale ecosystem model: Evaluation of temporal and spatial scaling issues in simulating soil thermal dynamics. *Journal of Geophysical Research*, *106*(D24), 33649–33670. https://doi.org/10.1029/2001jd900151